On the nonnormal–nonlinear interaction mechanism between counter-propagating Rossby waves

ARTICLE *in* THEORETICAL AND COMPUTATIONAL FLUID DYNAMICS · APRIL 2015

Impact Factor: 1.75 · DOI: 10.1007/s00162-015-0346-9

4 AUTHORS, INCLUDING:

Talia Tamarin
Weizmann Institute of Science
2 PUBLICATIONS **1** CITATION
SEE PROFILE

Eyal Heifetz
Tel Aviv University
57 PUBLICATIONS **511** CITATIONS
SEE PROFILE

Ron Yellin
Tel Aviv University
2 PUBLICATIONS **0** CITATIONS
SEE PROFILE

Theor. Comput. Fluid Dyn. (2015) 29:205–224
DOI 10.1007/s00162-015-0346-9

ORIGINAL ARTICLE

Talia Tamarin · Eyal Heifetz · Orkan M. Umurhan · Ron Yellin

On the nonnormal–nonlinear interaction mechanism between counter-propagating Rossby waves

Received: 14 May 2014 / Accepted: 23 March 2015 / Published online: 18 April 2015

Abstract The counter-propagating Rossby wave perspective to shear flow instability is extended here to the weakly nonlinear phase. The nonlinear action at a distance interaction mechanism between a pair of waves is identified and separated from the linear one. In the former, the streamwise velocity converges the far-field vorticity anomaly of the opposed wave, whereas in the latter, the cross-stream velocity advects the far-field mean vorticity. A truncated analytical model of two vorticity interfaces shows that higher harmonics generated by the nonlinear interaction act as a forcing on the nonnormal linear dynamics. Furthermore, an intrinsic positive feedback toward small-scale enstrophy results from the fact that higher harmonic pair of waves are generated in anti-phase configuration which is favored for nonnormal growth. Near marginal stability, the waves preserve their structure and numerical simulations of the weakly nonlinear interaction show wave saturation into finite amplitudes, in good agreement both with the fixed point solution of the truncated model, as well as with its corresponding weakly nonlinear Ginzburg–Landau amplitude equation.

Keywords Counter-propagating Rossby waves · Linear nonnormal and nonlinear interactions · Geophysical fluid dynamics

1 Introduction

The counter-propagating Rossby wave (CRW) is a concept that successfully rationalizes many aspects of linearized dynamics of shear flows. It was originally presented by Bretherton [1] in the context of atmospheric baroclinic instability, and after reviewed by Hoskins et al. [2], it received considerable attention as a conceptual tool to explain both baroclinic and barotropic instabilities (e.g., [3–11]). The essence of the Rossby wave counter-propagation mechanism and the modal and optimal nonmodal (nonnormal) CRW interaction are explained in [12] (hereafter HM05) and is summarized in Figs. 1 and 2 here.

Communicated by W. Dewar.

T. Tamarin (✉) · E. Heifetz · R. Yellin
Department of Geophysics, Atmospheric and Planetary Sciences, Tel Aviv University, Tel Aviv, Israel
E-mail: taliatamarin@hotmail.com

R. Yellin
E-mail: ronyellin@hotmail.com

E. Heifetz
Department of Meteorology, Stockholm University, Stockholm, Sweden
E-mail: eyalh@post.tau.ac.il

O. M. Umurhan
School of Natural Sciences, Applied Mathematics Unit, UC Merced, Merced, CA, USA
E-mail: orkan.umurhan@gmail.com

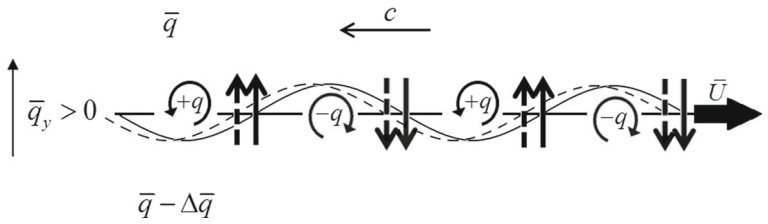

Fig. 1 Schematic illustration of the Rossby wave counter propagation mechanism over a cross-stream (y-direction) mean vorticity gradient (MVG) $\overline{q}_y$. The undulating *solid line* illustrates the CRW displacement. Positive and negative vorticity anomalies are indicated by $\pm q$, the circulation associated with them by *circled arrows* and the maximum cross-stream velocities (located a quarter wavelength out of phase of $\pm q$) by *solid arrows*. The cross-stream velocity associated with the perturbation advects the mean vorticity and as a result the wave propagates to the *left* (*dashed undulation*, the direction of propagation is indicated by a *horizontal arrow c*) relative to the mean flow (*bold arrow* $\overline{U}$). For counter-propagation, the signs of the mean flow and the MVG are the same (both are positive in this example)

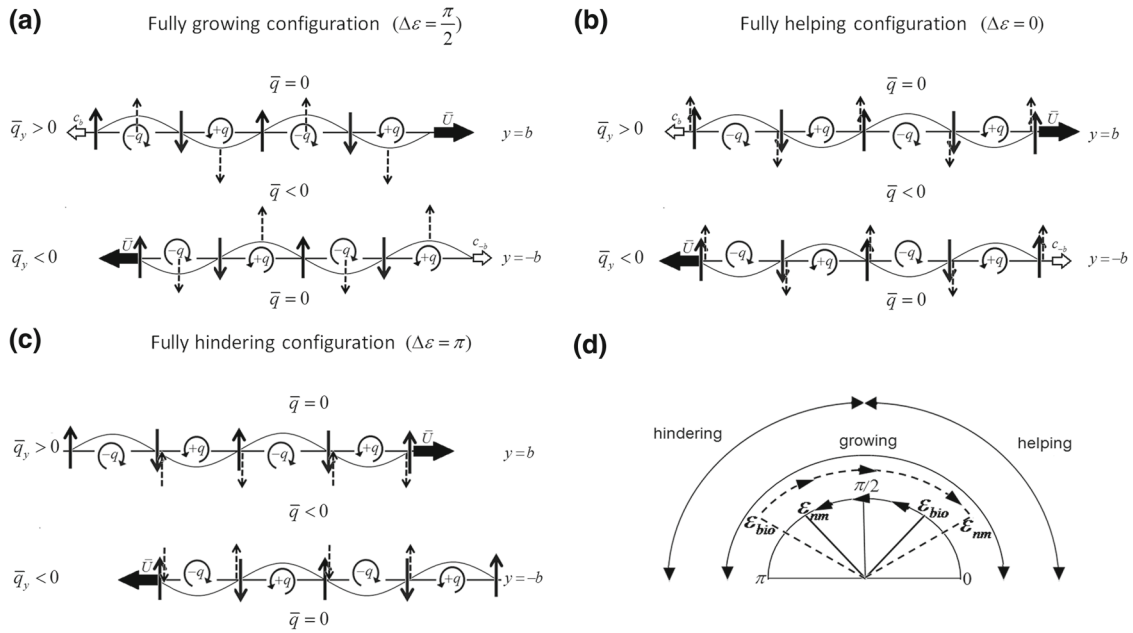

Fig. 2 Schematic description of the linear interactions between CRWs. **a** $\Delta\epsilon = \pi/2$, the crosswise velocities (*dashed arrows*) help to increase the vorticity anomaly of each CRW by advecting the mean flow, thereupon mutual transient growth is obtained. **b** $\Delta\epsilon = 0$, the cross-stream velocities interfere constructively so each CRW "helps" the other to counter-propagate faster, **c** $\Delta\epsilon = \pi$, the waves hinder each others' counter propagation, **d** Nonmodal growth in term of CRWs; ϵ_{nm} corresponds to the relative CRW phase difference in the growing normal mode configuration, while $\epsilon_{\text{bio}} = \pi - \epsilon_{nm}$ to its biorthogonal configuration. The maximal instantaneous growth occurs at $\epsilon = \pi/2$, while for $t \to \infty$, the initial and final optimal phases are symmetric with respect to $\pi/2$ (so $\epsilon(0) = \epsilon_{\text{bio}}$). Hence, when ϵ_{nm} is in the hindering/helping regime, the phase difference increases/decreases during optimal evolution (*solid/dashed arrows*)

The purpose of this study is to extend the understanding of CRW interaction to the nonlinear (NL) regime. NL Rossby wave interaction is an important mechanism in the evolution of central scenarios in atmospheric, oceanic and astrophysical fluid dynamics e.g., [13–17], yet, to the best of our knowledge, no explicit mechanistic CRW analysis exists to describe NL wave–wave interactions. In order to study the basic nature of the phenomenon, we choose a simple setup of a shear layer (Fig. 3 also known as the Rayleigh shear model [18]), in which CRW waves exist at the two edges of the shear layer. Since in the fully NL regime Rossby waves break into vortices, we consider here only interaction in the presence of strong enough damping that prevents vortex formation. Such damping may be related, for instance, to the Ekman boundary layer spin-down effect on the Rossby waves in the free atmosphere [19,20]. More generally, this study may be relevant to systems that are close to marginal stability, i.e., exhibit slight departures from marginality and are thus only weakly unstable (for example, filamentry vortex strip in the presence of an adverse shear [21]). The analysis therefore

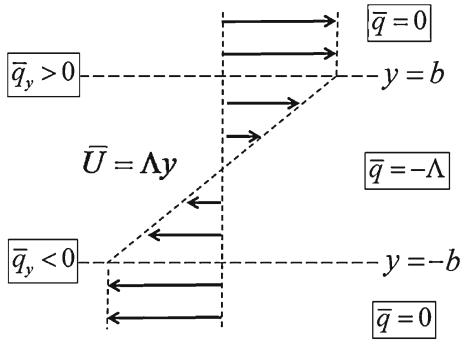

Fig. 3 The Rayleigh model, a piecewise linear velocity profile of a single shear layer with negative vorticity embedded by two infinite layers of zero vorticity. The *arrows* indicate mean streamwise velocities. At $y = \pm b$, the mean flow vorticity is discontinuous, yielding a positive/negative mean vorticity gradient at $y = \pm b$ (respectively)

focuses on the weakly NL phase; however, it is different from the triad interaction discussed in [22,23] in the absence of background shear.

The presence of shear makes the linearized dynamics to be nonnormal in the sense that the linearized eigenfunctions are generally nonorthogonal to each other and hence transient growth, obtained by singular value decomposition analysis (rather than by standard eigen value decomposition), may exceed the growth obtained by the most unstable mode. Hence these singular vectors are the first to interact nonlinearly. As mentioned above, the nonnormal CRW dynamics are described as well in HM05.

It is important to note that the analysis here is solely restricted to the CRW edge wave interaction. Thus interaction with continuous singular modes and the generation of critical layers [24], or weakly nonlinear description of vortex roll-up in shear layers [25], are beyond the scope of this paper.

The article is organized as follows. In Sect. 2, we formulate the NL CRW interaction into a truncated simplified model, and in Sect. 3, we describe the CRW mechanistic nonnormal–nonlinear feedback. In Sect. 4, we compare the truncated model to the results derived from the weakly NL Ginzburg–Landau amplitude equation and to direct numerical simulations. The results are concluded and discussed in Sect. 5.

2 Formulation

2.1 General formulation of plane parallel shear flows in terms of CRWs

We consider a 2D (streamwise, cross-stream) (x, y) incompressible barotropic flow with an equilibrated steady zonal mean shear flow, denoted by bars, and perturbations, denoted by primes: $\mathbf{u}(x, y, t) = \left[\overline{u}(y) + u'(x, y, t), v'(x, y, t)\right]$, so that the vorticity vector points in the z direction with magnitude $q(x, y, t) = \hat{\mathbf{z}} \cdot \nabla \times \mathbf{u} = \overline{q}(y) + q'(x, y, t) = -\frac{\partial \overline{u}}{\partial y} + \left(\frac{\partial v'}{\partial x} - \frac{\partial u'}{\partial y}\right)$. For simplicity, we represent damping by Rayleigh friction, $r = \tau_r^{-1}$, where τ_r is the relaxation time scale toward equilibrium. Given these model assumptions, the vorticity equation is:

$$\frac{\mathrm{D}q}{\mathrm{D}t} = \left(\frac{\partial}{\partial t} + \mathbf{u} \cdot \nabla\right) q = -r(q - \overline{q}). \tag{1}$$

This may be also written explicitly in terms of the mean flow and the perturbation, as:

$$\left(\frac{\partial}{\partial t} + \overline{u}\frac{\partial}{\partial x} + r\right) q' + v'\frac{\partial \overline{q}}{\partial y} = -\nabla \cdot (\mathbf{u}'q'), \tag{2}$$

where the LHS and RHS represent the linear and the nonlinear components, respectively. In order to express the perturbation velocity field in terms of the perturbation vorticity, we apply first a streamwise Fourier decomposition: $q'(x, y, t) = \int_{-\infty}^{\infty} q_k(y, t)\mathrm{e}^{ikx}\mathrm{d}k$, where $q_k = \frac{1}{2}Q_k\mathrm{e}^{i\epsilon_k} = q^*_{-k}$ (asterisk denotes the complex conjugate), so that $q' = \int_0^{\infty} Q_k(y, t)\cos[kx + \epsilon_k(y, t)]\mathrm{d}k = \int_0^{\infty} \tilde{q}_k \mathrm{d}k$. $Q_k(y, t)$ and $\epsilon_k(y, t)$, can be therefore regarded as the respected amplitude and phase of the vorticity kernel $\tilde{q}_k(x, y, t)$. The perturbation velocity

field associated with such a vorticity kernel is obtained by the Green function of the stream-function ψ, where $\mathbf{u}' = \hat{\mathbf{z}} \times \nabla\psi' = \left[-\frac{\partial\psi'}{\partial y}, \frac{\partial\psi'}{\partial x}\right]$, $q' = \frac{\partial v'}{\partial x} - \frac{\partial u'}{\partial y} = \nabla^2\psi'$, and therefore $\tilde{q}_k(y,t) = -k^2\tilde{\psi}_k + \frac{\partial^2\tilde{\psi}_k}{\partial y^2}$. Hence, for open flows,

$$\psi'(x,y,t) = \int_0^\infty \left[\int_{-\infty}^\infty Q_k(y_0,t)\cos[kx + \epsilon_k(y_0,t)]G_k(y,y_0)\mathrm{d}y_0\right]\mathrm{d}k = \int_0^\infty \tilde{\psi}_k \mathrm{d}k, \tag{3}$$

where $G_k(y,y_0) = -\mathrm{e}^{-k|y-y_0|}/2k$ is the Green function satisfying $\nabla^2 G_k(y,y_0) = \delta(y-y_0)$, together with the boundary conditions of vanishing velocities at $(-\infty,\infty)$ (For closed, or semi-closed, boundaries, the suitable Green functions appear in the Appendix of HM05). The velocity perturbations are therefore

$$u'(x,y,t) = \int_0^\infty \left[\int_{-\infty}^\infty -Q_k(y_0)\cos[kx + \epsilon_k(y_0)]\frac{\partial G_k}{\partial y}\mathrm{d}y_0\right]\mathrm{d}k = \int_0^\infty \tilde{u}_k \mathrm{d}k, \tag{4a}$$

$$v'(x,y,t) = \int_0^\infty \left[\int_{-\infty}^\infty kQ_k(y_0)\sin[kx + \epsilon_k(y_0)]G_k dy_0\right]\mathrm{d}k = \int_0^\infty \tilde{v}_k \mathrm{d}k, \tag{4b}$$

representing the appropriate vorticity inversion. Each localized vorticity kernel $\tilde{q}_k(y_0)$ is associated with a far-field velocity $\tilde{\mathbf{u}}_k(y,y_0)$, where $\tilde{u}_k$ is in (out of) phase below (above) $\tilde{q}_k$, and $\tilde{v}_k$ leads $\tilde{q}_k$ by a quarter wavelength (as sketched schematically by the circled arrows in Fig. 1). Equation (2), in spectral form, now appears as:

$$\begin{aligned}\int_{k=0}^\infty \frac{\partial\tilde{q}_k}{\partial t}\mathrm{d}k = &-\int_{k=0}^\infty \left[\left(\overline{u}\frac{\partial}{\partial x} + r\right)\tilde{q}_k + \tilde{v}_k\frac{\partial\overline{q}}{\partial y}\right]\mathrm{d}k \\ &-\int_{k_1=0}^\infty\int_{k_2=0}^\infty \nabla\cdot(\tilde{\mathbf{u}}_{k_1}\tilde{q}_{k_2})\delta\Big(k_1 \pm k_2 = k\Big)\mathrm{d}k_1\mathrm{d}k_2,\end{aligned} \tag{5}$$

where $\delta(k_1 \pm k_2 = k)$ represents streamwise triad interactions. Hence, for a specific spectral component (5) can be written symbolically as:

$$\begin{aligned}&\frac{\partial\tilde{q}_k}{\partial t} = \mathbf{NN}_k\{\tilde{q}_k\} + \mathbf{NL}_{(k_1\pm k_2=k)}\{\tilde{q}_{k_1}\tilde{q}_{k_2}\}, \Longrightarrow \\ &\tilde{q}_k(t) = \mathrm{e}^{\mathbf{NN}_k t}\tilde{q}_k(0) + \int_0^t \mathrm{e}^{\mathbf{NN}_k(t-\tau)}\mathbf{NL}_{(k_1\pm k_2=k)}\{\tilde{q}_{k_1}\tilde{q}_{k_2}\}(\tau)\mathrm{d}\tau.\end{aligned} \tag{6}$$

The linearized operator is generally nonnormal (**NN**) due to the mean shear differential advection, and the nonlinear (**NL**) contribution results from the triad interaction. Equation (6) suggests that the latter can be interpreted as a continuous temporal forcing on the nonnormal linear dynamics. The triad generation of $\mathbf{NL}_{(k_1\pm k_2=k)}$ at time τ evolves linearly in the time increment between τ and the present time t, in a nonnormal fashion. Obviously, the triad interactions $(k - k_2 = k_1)$ and $(k - k_1 = k_2)$ affect back on (k_1, k_2), hence a nonlinear–nonnormal feedback is an intrinsic feature in the dynamics. This feedback was summarized by Baggett and Trefethen [26]: Initially, small perturbations grow linearly where some structures experience a significant transient growth due to nonnormality. When they grow further, nonlinearity becomes important and new wavenumbers with new structures are generated by triad interaction ("nonlinear mixing"). Some of these new structures experience nonnormal transient growth, inducing further nonlinear feedback, and so forth.

2.2 CRWs in the Rayleigh model

We consider the simple Rayleigh model basic state sketched schematically in Fig. 3 that supports the existence of CRW pairs on the two sides of the shear layer:

$$\bar{u}(y) = \begin{cases}\Lambda b & y \geq b \\ \Lambda y & -b \leq y \leq b; \\ -\Lambda b & y \leq -b,\end{cases} \qquad \bar{q}(y) = \begin{cases}0 & y > b \\ -\Lambda & -b < y < b; \\ 0 & y < -b\end{cases} \tag{7}$$

$$\frac{\partial\bar{q}}{\partial y} = \Lambda[\delta(y-b) - \delta(y+b)].$$

Since $\frac{\partial \bar{q}}{\partial y}$ is concentrated in two δ-functions at $y = \pm b$, Eq. (2) suggests that the vorticity perturbation should be as well concentrated there as δ-functions; $q'(x, y, t) = \hat{q}^b(x, t)\delta(y - b) + \hat{q}^{-b}(x, t)\delta(y + b)$. Hence, by integrating (2) in y between $(\pm b - \varepsilon, \pm b + \varepsilon)$, where $\varepsilon \to 0$, the nonlinear cross-stream vorticity flux convergence, $-\frac{\partial(v'q')}{\partial y}$, vanishes[1] and (2) reduces at $y = \pm b$ to

$$\left(\frac{\partial}{\partial t} \pm \Lambda b \frac{\partial}{\partial x} + r\right) \hat{q}^{\pm b} \pm v'\Lambda = -\frac{\partial(u'\hat{q}^{\pm b})}{\partial x}. \tag{8}$$

As far as remote CRW interactions are concerned, the cross-stream perturbation velocity affects the linear dynamics by advecting the mean flow *at a distance* [i.e., the last term in the LHS of Eq. (8)], while the streamwise velocity perturbation affects the nonlinear dynamics by converging the perturbation vorticity of the opposing CRW [the term in the RHS of Eq. (8)]. Writing then

$$\begin{aligned} \tilde{q}_k &= \hat{q}_k^b(x, t)\delta(y - b) + \hat{q}_k^{-b}(x, t)\delta(y + b) \\ &= \hat{Q}_k^b(t) \cos\left[kx + \epsilon_k^b(t)\right]\delta(y - b) + \hat{Q}_k^{-b}(t) \cos\left[kx + \epsilon_k^{-b}(t)\right]\delta(y + b), \end{aligned} \tag{9}$$

and substitute in (3), the stream-function and velocities take the form:

$$\tilde{\psi}_k = -\frac{1}{2k}\left[\hat{q}_k^b \mathrm{e}^{-k|y-b|} + \hat{q}_k^{-b}\mathrm{e}^{-k|y+b|}\right], \tag{10a}$$

and the velocity fields at the interfaces are

$$\tilde{u}_k^{\pm b} = \mp\frac{1}{2}\hat{q}_k^{\mp b}\mathrm{e}^{-2kb}, \tag{10b}$$

and

$$\tilde{v}_k^{\pm b} = -\frac{1}{2k}\left[\frac{\partial \hat{q}^{\pm b}}{\partial x} + \frac{\partial \hat{q}^{\mp b}}{\partial x}\mathrm{e}^{-2kb}\right]. \tag{10c}$$

2.3 Truncated model

We assume an initial small perturbation of wavenumber k which first grows linearly [according to the LHS of (8)] and when it becomes large enough generates nonlinearly, [according to the RHS of (8)], perturbation in wavenumber $2k$ ($k + k = 2k$). The latter interacts back with wavenumber k. The mutual $k \Longleftrightarrow 2k$ equations describing this process are (see "Appendix A" for a detailed derivation):

$$\dot{Q}_k = \left\{[\sigma_k \sin(\Delta\epsilon_k) - r] - \frac{k}{2}\sigma_k Q_{2k} \sin\left(\frac{\Delta\epsilon_{2k}}{2}\right)\right\} Q_k, \tag{11a}$$

$$\dot{\Delta\epsilon}_k = 2\sigma_k\left[\cos(\Delta\epsilon_k) - f_k\right] + k\sigma_k Q_{2k} \cos\left(\frac{\Delta\epsilon_{2k}}{2}\right), \tag{11b}$$

$$\dot{Q}_{2k} = \left\{[\sigma_{2k} \sin(\Delta\epsilon_{2k}) - r] + k\sigma_k \frac{Q_k^2}{Q_{2k}} \sin\left(\frac{\Delta\epsilon_{2k}}{2}\right)\right\} Q_{2k}, \tag{12a}$$

$$\dot{\Delta\epsilon}_{2k} = 2\sigma_{2k}\left[\cos(\Delta\epsilon_{2k}) - f_{2k}\right] + 2k\sigma_k \frac{Q_k^2}{Q_{2k}} \cos\left(\frac{\Delta\epsilon_{2k}}{2}\right). \tag{12b}$$

For the NL interaction, the scale of the vorticity matters. Recall that Q is the vorticity density amplitude (with units of speed), hence the scaling of (11) and (12) indicates that Q is normalized as well by $2\Lambda b$. In the linear

[1] This is supported by the numerical simulations presented in Section 4, where the mean vorticity gradients are concentrated in two narrow, but finite bands. There the terms $\int_{\pm b-\varepsilon}^{\pm b+\varepsilon} \frac{\partial(v'q')}{\partial y}\mathrm{d}y$, are indeed smaller by at least two orders of magnitude than $\int_{\pm b-\varepsilon}^{\pm b+\varepsilon} \frac{\partial(u'q')}{\partial x}\mathrm{d}y$.

approximation, $Q^{\pm b}$ represent the CRW vorticity anomalies at the edges, associated with the cross-stream displacement $\eta'^{\pm b} = -[q'/\frac{\partial \overline{q}}{\partial y}]^{\pm b} = \mp q^{\pm b}/\Lambda$. Since an implicit assumption in the CRW description is that these displacements are localized, we set the damping to allow a maximum value of $Q = 0.5$, corresponding to a CRW displacement amplitude of half of the shear layer's width. Within this constraint, system (11, 12) admits stable fixed points ("Appendix B"). Although the system is not closed in the sense that other harmonics may interact with $(k, 2k)$, it will be shown that if k is taken as the wavenumber of the most unstable mode, these fixed points provide a good approximation for the saturated state when compared to straightforward wave–wave simulations and to the derivation of the weakly nonlinear Landau–Ginzburg amplitude equation.

3 Nonlinear–nonnormal CRW feedback

3.1 Mechanistic description

Equations (11–12) can be written equivalently in the form of (6)

$$\tilde{\mathbf{q}}_k = Q_k \begin{pmatrix} e^{i\epsilon_k^b} \\ e^{i\epsilon_k^{-b}} \end{pmatrix}; \quad \mathbf{NN}_k = -i \begin{pmatrix} kc_k^b - ir & -\sigma_k \\ \sigma_k & kc_k^b - ir \end{pmatrix}, \tag{13}$$

in which,

$$\mathbf{NL}_{(k+k=2k)} \equiv \mathbf{NL}_{2k} = ik\sigma_k Q_k^2 e^{i\left(\epsilon_k^b + \epsilon_k^{-b}\right)} \begin{pmatrix} 1 \\ -1 \end{pmatrix}, \tag{14a}$$

$$\mathbf{NL}_{(2k-k=k)} \equiv \mathbf{NL}_k = i\frac{k}{2}\sigma_k Q_k Q_{2k} \begin{pmatrix} e^{i\left(\epsilon_{2k}^b - \epsilon_k^{-b}\right)} \\ -e^{i\left(\epsilon_{2k}^{-b} - \epsilon_k^b\right)} \end{pmatrix}, \tag{14b}$$

so that

$$\dot{\tilde{\mathbf{q}}}_\mathbf{k} - \mathbf{NN}_k \tilde{\mathbf{q}}_k = \mathbf{NL}_k; \qquad \dot{\tilde{\mathbf{q}}}_\mathbf{2k} - \mathbf{NN}_{2k} \tilde{\mathbf{q}}_{2k} = \mathbf{NL}_{2k} \Longrightarrow \tag{15}$$

$$\tilde{\mathbf{q}}_k(t) = e^{\mathbf{NN}_k t} \tilde{\mathbf{q}}_k(0) + \int_0^t e^{\mathbf{NN}_k (t-\tau)} \mathbf{NL}_k(\tau) d\tau, \tag{16a}$$

$$\tilde{\mathbf{q}}_{2k}(t) = e^{\mathbf{NN}_{2k} t} \tilde{\mathbf{q}}_{2k}(0) + \int_0^t e^{\mathbf{NN}_{2k} (t-\tau)} \mathbf{NL}_{2k}(\tau) d\tau. \tag{16b}$$

The NL CRW interaction at a distance, the RHS of (8), arises from the convergence of vorticity flux of each CRW. The convergence is brought about by the induced streamwise velocity of the opposing wave (Recall that the streamwise velocity of a CRW changes sign on the two sides of its "home base" (HM05) and, hence, its self contribution to the streamwise velocity there is zero). Equation (14a) indicates that this interaction, when resulting from a pair of CRWs of the same wavenumber k ($\mathbf{NL}_{(k+k=2k)}$), generates a pair of CRWs of wavenumber $2k$ which are always exactly anti-phased ($\Delta\epsilon_{2k} = \pi$). This anti-symmetry is simply because positive (negative) vorticity anomalies are associated with positive (negative) streamwise velocity below (above) them (Fig. 4a). Equation (12b) shows, in turn, that when the generated CRW $2k$ pair is in anti-phase at some instant moment, $\dot{\Delta}\epsilon_{2k} < 0$ for every nonzero k (since $f_{2k} > -1$ and $\cos(\frac{\pi}{2}) = 0$). The linear term is negative because when the CRWs are out of phase, they fully hinder each other's counter-propagation rate, hence they cannot resist the shear and their mutual phase difference reduces. Consequently, the NL term in (12b) becomes negative as well ($\cos(\frac{\Delta\epsilon_{2k}}{2}) < 0$ for $\Delta\epsilon_{2k} < \pi$) Hence, the $2k$ CRW mode will be shifted into the growing regime (Fig. 4b). Equation (16b) indicates that each CRW pair of wavenumber $2k$, generated in anti-phase at some instant of time $t = \tau$, is subject to nonnormal linear evolution for those times $\tau < t < t_{\text{now}}$ (i.e., for the stretch of time $\Delta t = t_{\text{now}} - \tau$). Since the linear evolution shifts the CRW phase into the growing regime, the accumulated effect of the $k + k \Leftrightarrow 2k$ NL interaction is therefore to increase the enstrophy deposited into the $2k$ mode. The backward $2k \Rightarrow k$ NL interaction ($\mathbf{NL}_{(2k-k=k)}$) is more complex since it involves different harmonics within the CRW pairs. It is clear, however, that the signs of the NL terms in (11a) and (12a) are opposite. Hence while Q_{2k}^2 grows due to NL interaction, Q_k^2 correspondingly decays.

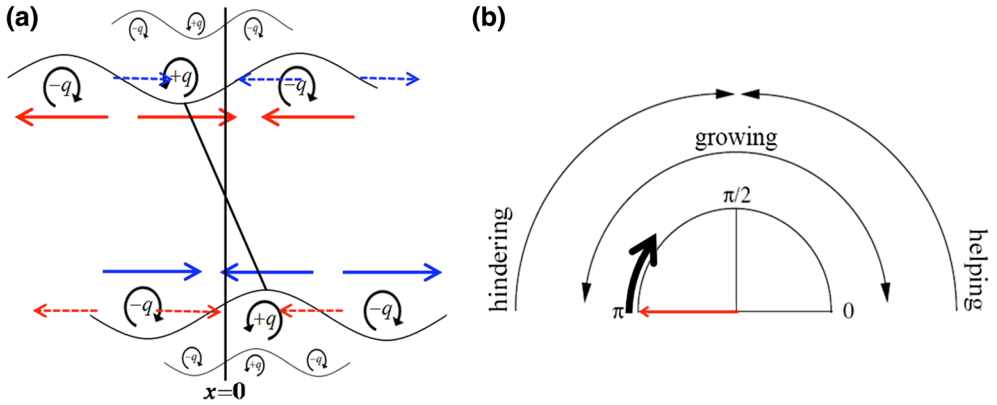

Fig. 4 **a** A schematic illustration of the nonlinear CRWs interaction. The *blue* (*red*) *arrows* indicate the streamwise velocities associated with the lower (upper) CRW of wavenumber k, where *solid arrows* represent velocities at the CRW "home base" and *dashed arrows* on the opposed edge. The nonlinear zonal vorticity flux divergence/convergence results in a new pair of wavenumber $2k$, created exactly in anti-phase. **b** Evolution of the phase difference between the two CRWs of wavenumber $2k$. Since they are generated in anti-phase, which is a fully hindering configuration, the shear acts to decrease the phase difference and consequently the CRWs enter into the growing regime

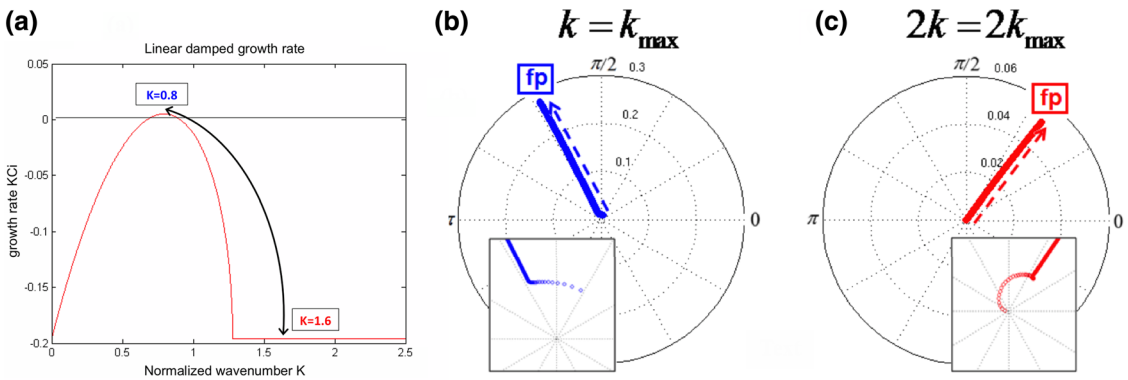

Fig. 5 **a** Linear damped normalized growth rate. The *black arrow* indicates the relevant modes of interaction; the most unstable NM $k_{\max} = 0.8$, which is weakly unstable, and its double harmonic $2k_{\max} = 1.6$ which is heavily damped. **b, c** show the phase and amplitude evolution for $k_{\max}$ and $2k_{\max}$, respectively, in polar coordinates $(Q(t), \Delta\epsilon(t))$ (see the *box* of enlarged area near the origin). The *dashed arrows* show the direction of the evolution, pointing toward the fixed point steady-state solution. **b** $k_{\max} = 0.8$ is initiated from the biorthogonal phase $\Delta\epsilon_{0.8}{}^{\text{bio}} \approx 0.35\pi$ with a small amplitude ($\approx$0.01). The mode initially exhibits linear nonmodal growth; however, instead of growing indefinitely, it saturates to $Q_{0.8}^{\text{fp}} \approx 0.27$ and $\Delta\epsilon_{0.8}^{\text{fp}} \approx 0.65\pi$. **c** $2k_{\max} = 1.6$ is initiated with zero amplitude. Although linearly damped, it manages to grow significantly and finally saturates at $Q_{1.6}^{\text{fp}} \approx 0.05$ with $\Delta\epsilon_{1.6}^{\text{fp}} \approx 0.29\pi$

3.2 Example of $k \Longleftrightarrow 2k$ feedback

One of the most straightforward examples of this $k \Longleftrightarrow 2k$ feedback is when k is taken to be the most unstable mode of the linear dynamics and the system is damped to be in the weakly nonlinear regime. The undamped system described in HM05 picks its most unstable mode at $k_{\max} = 0.8$, with a growth rate of 0.201. By taking $r = 0.197$, the effective growth rate of $k_{\max}$ becomes $kc_i = 0.004$ (2 % of the undamped growth rate). For such damping, the mode of $2k_{\max} = 1.6$ (which is neutral in the undamped case) has a negative exponential modal growth rate of approximately -0.2 (Fig. 5a). If we restrict our thinking to purely normal mode dynamics, it is (at first glance) somewhat surprising that the $2k_{\max}$ mode may affect the $k_{\max}$ one—instead of being purely slaved to it. In order to examine the interaction between these two modes, we time advance numerically equations (16) using third-order Adams–Bashforth method. We initiate the system with a pure wave corresponding to the most unstable mode, with a small amplitude $Q_{k_{\max}} = 0.01$ and a phase difference corresponding to the bi-orthogonal vector $\Delta\epsilon^{\text{bio}} = \pi - \Delta\epsilon^{\text{NM}} = 0.36\pi$ (which is the optimal nonnormal configuration for large target times). The evolution of the system toward steady state is presented in Fig. 5b, c

in polar coordinates $(Q(t), \Delta\epsilon(t))$ for both $k_{\max}$ and $2k_{\max}$. At the initial stage of the evolution, $Q_{k_{\max}}$ grows in a nonnormal fashion while $\Delta\epsilon_{k_{\max}}$ increases and crosses $\pi/2$, as expected (small box of Fig. 5b). However, the backward interaction $2k_{\max} \Leftarrow k_{\max}$ prevents the vorticity at $k_{\max}$ to grow indefinitely and it eventually balances the linear growth, and consequently the vorticity converges to the fixed point value of (B1a, B2a) (giving $Q^{\text{fp}}_{k_{\max}} \approx 0.27$, $\Delta\epsilon^{\text{fp}}_{k_{\max}} \approx 0.65\pi$). The final phase is slightly larger than the normal mode one due to the NL term in (11b) which is small but positive.

The growth of $2k_{\max}$ mode due to the NL $k_{\max} \Rightarrow 2k_{\max}$ interaction is effective enough to overcome the strong linear damping since it keeps seeding CRW pairs π out of phase, which are then immediately shifted by the shear into the growing regime (as in Fig. 4b). Since $\tilde{\mathbf{q}}_{2k}(0) = 0$ in this example, $\tilde{\mathbf{q}}_{2k}(t)$ depends only on the accumulated contribution of the CRWs, seeded by the NL interaction, which then evolve nonnormally during the increment $t - \tau$ (16b). When the CRWs have equal amplitudes, the linearly interacting $2k_{\max}$ CRWs have no fixed modal phase locking. Nevertheless, here the CRW pair saturates eventually into the phase-locked configuration predicted by (B1a), $\Delta\epsilon^{\text{fp}}_{2k_{\max}} \approx 0.29\pi$ (Fig. 5c).

This can be understood in the following mechanistic way from the nonlinear $k_{\max} \Rightarrow 2k_{\max}$ interaction. CRW pairs generated nonlinearly at time τ close to present will have a phase difference close to π, but will also have relatively small amplitudes; CRW pairs that are generated at some previous time τ will have more time to grow and to be shifted toward smaller phase differences while crossing $\pi/2$; CRW pairs generated close to the initial time may already be in the decaying regime (phase difference smaller than zero) and therefore will have small amplitudes. Hence, the most significant contribution to the integral at the RHS of (16b) comes from the CRWs which have large amplitudes but small positive phase differences. This is consistent with the fixed point solutions (B1a, B2a) found for $2k_{\max}$, which describe the overall accumulated contribution in steady state.

The amplitude evolution for both $k_{\max}$, $2k_{\max}$ is plotted as a function of time in Fig. 7 (dashed blue and red lines, respectively). As can be seen, the amplitudes initially grow exponentially but eventually saturate at fixed finite amplitudes, given by the fixed point solutions (B1a, B2a) as was described above. The rest of the results presented in Fig. 7 will be discussed in the following sections.

4 Comparison of the truncated model

4.1 Weakly NL Ginzburg–Landau model

We wish now to compare the CRW truncated model with a standard derivation of a Ginzburg–Landau amplitude equation (GLAE). This procedure differs from the analysis above since it works with weakly unstable normal modes and is meant to describe time-asymptotic behavior without taking explicit consideration of transient growth dynamics. Furthermore, the NL dynamics described in GLAE is the result of both wave–mean flow and wave–wave interaction. Since in this work we focus on the Rossby NL wave–wave interaction mechanism, we exclude the wave–mean flow dynamics in the derivation of the GLAE. This, in a sense, compliments the work of Pedlosky [13] who analyzed the (baroclinic) Rossby GLAE resulted solely from wave–mean flow interaction.

Close to marginality, the modal growth rate has the approximated upside-down parabola structure (Fig. 5a),

$$\sigma = kc_i \approx (r_c - r) - b(k - k_{\max})^2, \tag{17}$$

where r_c is the critical damping required to prevent modal instability to exist (hence, r_c is equal to the most unstable inviscid growth rate), $b \equiv -\frac{1}{2}\left(\frac{\partial^2\sigma}{\partial k^2}\right)_{k=k_{\max}} > 0$ (and $\left(\frac{\partial\sigma}{\partial k}\right)_{k=k_{\max}} = 0$). Since the departure from marginality is small, we can define ϵ as a small parameter so that $(k - k_{\max}) \equiv \epsilon\delta k$, and accordingly $(r_c - r) \equiv \epsilon^2\delta r$. The derivation of the GLAE for our case is detailed in ("Appendix C"). Eventually, we arrive at an amplitude equation of the form:

$$\frac{\partial A}{\partial T} = \delta r A - \beta_{2\text{k}} A|A|^2, \tag{18}$$

where A is the amplitude of the $k_{\max}$ wave (the modal linear dynamics is recovered by $\frac{\partial A}{\partial T} = \delta r A$). $T \equiv \epsilon^2 t$ is the slow time scale and $\beta_{2\text{k}}$ is the nonlinear parameter representing the NL attenuation due to the $k_{\max} \Longleftrightarrow 2k_{\max}$ interaction. For the damping value used in Fig. 5, we obtain $\beta_{2k} = 0.264$.

In Fig. (7), we plot the time development of the vorticity amplitude for $(k_{\max}, 2k_{\max})$ resulting from (18) (blue and red star lines) together with the evolution determined from our truncated CRW model (dashed lines)

and direct numerical simulation (solid line) discussed in the next subsection. The final saturation amplitudes obtained from the GLAE are translated to ($Q^{LG}_{k_{\max}} \approx 0.24$, $Q^{LG}_{2k_{\max}} \approx 0.06$) which stand in very good agreement with the corresponding fixed point solution of the truncated CRW model ($Q^{\mathrm{fp}}_{k_{\max}} \approx 0.27$, $Q^{\mathrm{fp}}_{2k_{\max}} \approx 0.05$).

4.2 Direct numerical simulations

Another way to examine the validity of the CRW truncated model is to compare it with results from direct numerical simulations. We use the smooth profile

$$\overline{U} = \frac{\Lambda\delta}{2}\left[\log\left(\cosh\left(\frac{y+1}{\delta}\right)\right) - \log\left(\cosh\left(\frac{y-1}{\delta}\right)\right)\right], \tag{19}$$

in which δ controls the tightness of the transition zones representing the step function form of the mean vorticity. Taking $\delta = 0.05$ and keeping the same normalization as defined in Section 2.3, we employ a pseudo-spectral code (e.g., [27]) to solve the nonlinear equations of motion.[2]

In order to perform a meaningful comparison with the truncated CRW model in which wave-mean flow interaction is absent, we run a series of numerical experiments in which the mean state is held fixed.[3] We initially perturb the flow with some small random noise, with vorticity values at the order of $O(10^{-3})\Lambda$. The dynamical evolution is presented in Fig. 6. We plot a series of snapshots at different normalized times $t = 500, 1500, 1700, 2500$, where we show the total vorticity (top panel), the perturbation vorticity (middle panel) and the streamwise discrete Fourier transform (DFT) of the perturbation (lower panel). As is evident from Fig. 6a, at the initial linear regime ($t = 500$), the most unstable mode $n = 2$ emerges. The perturbation vorticity appears as a perfect sinusoidal wave, and its structure is tilted against the shear in a hindering-growing configuration (in agreement with the linear theory). The calculated growth rate matches the linear one, as expected. Later on at $t = 1500$ (Fig. 6b), the sinusoidal perturbation slowly distorts as the perturbation grows and the double-harmonic ($n = 4$) appears. At this stage of the dynamics, the growth rate of the $n = 2$ mode begins to decrease as the perturbation of the double-harmonic $n = 4$ begins to grow. This evolution stands in agreement with the truncated model. At $t = 1700$, Fig. 6c, the $k + 2k = 3k$ interaction emerges and the harmonic $n = 6$ appears. This interaction is not represented in our truncated model. Eventually during the saturation stage at $t = 2500$, even higher harmonics are excited. Nevertheless, as is shown in Fig. 7, the evolution of the ($k_{\max}$, $2k_{\max}$) amplitudes is in overall agreement with the truncated model, as well as with the GLAE (although the transition to the saturated stage in the simulation that occurs at $t \approx 1850$ is more abrupt). The final amplitude values in the simulation at saturation are ($Q^{\mathrm{sat}}_{k} \approx 0.38$, $Q^{\mathrm{sat}}_{2k} \approx 0.07$).

5 Discussion and Conclusions

In many central geophysical fluid dynamical setups, such as in the synoptic (Rhines) scale of the mid-latitude troposphere, where the weather is highly variable, jets, Rossby waves and vortices coexist. Rossby waves grow linearly via baroclinic instability in a nonnormal transient fashion on the expense of the sheared jet and then deposit back part of their energy to the mean jet via nonlinear barotropic processes. Rossby waves interact as well nonlinearly between themselves and break into vortices (e.g., [29]). Obviously, such scenarios are highly complex. Nonetheless, for the linearized dynamics, simplified toy models (such as Eady [30], Carney [31], Phillips [32] and Rayleigh [18]) were found valuable in explaining much of the essence of the dynamics, especially the concepts of the mechanism of linearized growth of Rossby waves on the expense of the sheared jets. These understandings serve as guiding tools when analyzing and rationalizing more realistic scenarios. Furthermore, simplified quasi-NL wave–mean flow interaction models exist to describe the combined

[2] The equations are solved using standard Fourier spectral methods [28], with a spatial resolution of 256×512 grid points in the (x, y) directions, respectively. The model is periodic in x and y. As such, we adopt a mean vorticity profile $\bar{q}$ which is also periodic on the meridional scale L_y. With large values of L_y compared to the shear layer width $L_y = L_x = 2\lambda_{\max}$ (thus the most unstable mode has a quantized wavenumber $n = 2$). The normalized damping r is chosen so that the linear growth rate would be the same as in the truncated nonlinear interaction ($kc_{i\,\max} \approx 0.004$). The dynamics in our numerical experiment mimic the infinite Rayleigh model to a very good approximation. We use hyper viscosity proportional to ∇^8 and impose the typical 2/3 dealiasing rule. The solution is advanced in time by a third-order Adams–Bashforth scheme.

[3] In practice, it means automatically setting equal to zero all nonlinearities generating power into $k_x = 0$ modes, as well as vanishing the damping coefficient r operating on these modes.

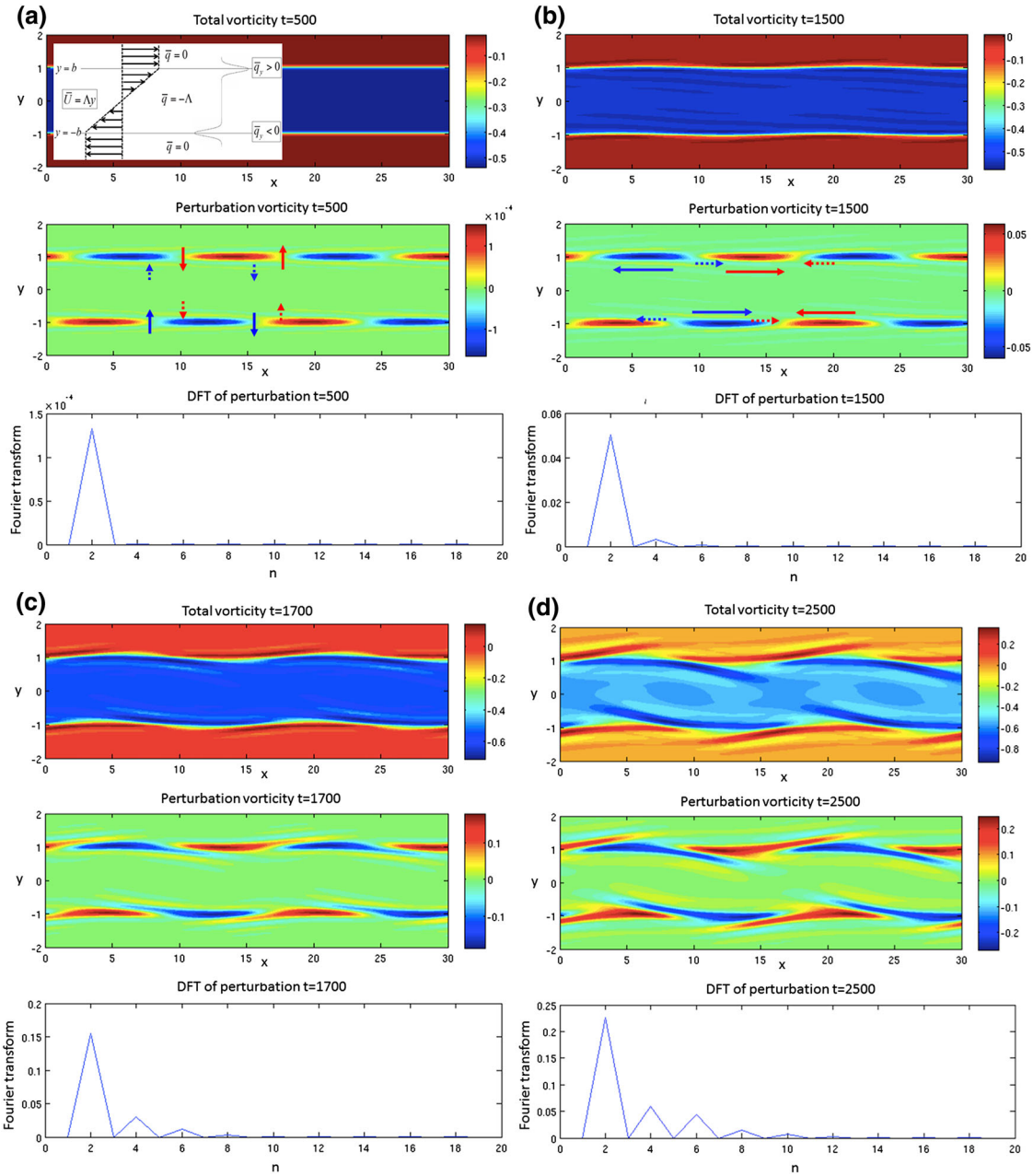

Fig. 6 Snapshots at selected times of the CRW evolution ($t = 500, 1500, 1700, 2500$), showing the total vorticity (*top*), the perturbation vorticity (*middle*) and the streamwise discrete Fourier transform (DFT) of the perturbation (*lower*). **a** $t = 500$. *Top* the schematic Rayliegh profile is added to the total vorticity field for reference. *Middle* evidently the most unstable mode has emerged and is tilted against the shear. The *red* (*blue*) *arrows* demonstrate the cross-stream velocities associated with positive (negative) vorticity anomalies, illustrating the linear growth mechanism. *Bottom* DFT of this perturbation shows that $n = 2$ is indeed the dominant mode. **b** $t = 1500$. *Top and middle* the perturbation grows and the total vorticity field starts to be distorted. The *red* (*blue*) *arrows* demonstrate the streamwise velocities associated with positive (negative) vorticity anomalies, illustrating the nonlinear wave–wave interaction. *Bottom* the double harmonic $n = 4$ begins to emerge. **c** $t = 1700$. *Top* as the perturbations keep growing, the total vorticity field becomes more distorted. *Middle* the sinusoidal perturbation slowly distorts as the perturbation grows and other harmonics appear. *Bottom* the double harmonic $n = 4$ grows further and the $n = 6$ harmonic begins to appear. **d** $t = 2500$. *Top and middle* the saturated steady state of the system. *Bottom* higher-order harmonics are eventually excited as well due to nonlinear triad interactions

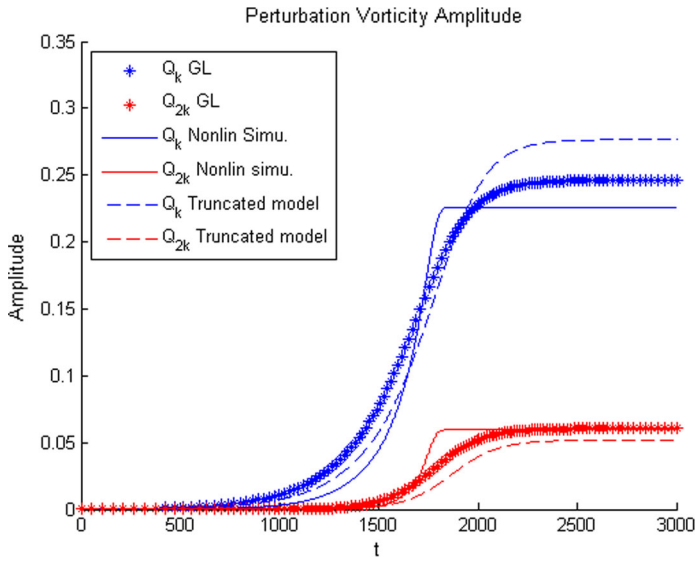

Fig. 7 Time development of the CRWs vorticity amplitude for $k_{\max}$ (*blue*) and $2k_{\max}$ (*red*), as determined from the weakly nonlinear truncated model (*dashed lines*), the Ginzburg–Landau amplitude equation (*star lines*) and the direct numerical simulation (*solid lines*). Overall, we obtain a good agreement between the three methods. All exhibit an exponential growth during the linear stage, followed by a nonlinear saturation to finite amplitudes that occur roughly at the same time, with similar final saturated amplitudes

baroclinic and barotropic equilibration (e.g., [33,34]) between Rossby waves and the jets; however, to the best of our knowledge, no equivalent models exist to describe the fundamental mechanism of Rossby wave–wave interaction in the presence of shear flow. We regard the study here as a first step in this direction. Thus, the model is not aimed to describe a realistic setup but rather to provide a platform to study the Rossby wave–wave interaction.

In this model, the linear and the NL CRW interaction mechanisms were found to be cleanly separated. The linear interaction is via the cross-stream velocity, while the NL one is via the streamwise velocity. The latter converges the vorticity perturbation of the remote CRW in a way that a CRW pair of the same wavenumber k is continuously seeding anti-phased CRW pairs in wavenumber $2k$. Since an anti-phase configuration is a fully hindering one, these newly generated $2k$ CRW pairs are immediately shifted by the shear (in a nonnormal fashion) into their growing regime. On the contrary, the backward interaction $k \Leftarrow 2k$ acts generally to decay the CRW pair of wavenumber k. This understanding is suggestive and may shed light upon the mechanism that triggers systematic direct enstrophy cascade in 2D shear flows.

In the weakly nonlinear regime, such $k \Longleftrightarrow 2k$ interaction can lead to a wave–wave saturated equilibrium between the CRW pairs of k and $2k$. For strong enough damping, the most unstable mode $k_{\max}$ is only slightly unstable, and the $2k_{\max}$ one is heavily damped. Nevertheless, the $k_{\max} \Rightarrow 2k_{\max}$ interaction is efficient enough to resist the strong linear damping of $2k_{\max}$, while the $k_{\max} \Leftarrow 2k_{\max}$ interaction decreases efficiently the linear growth of $k_{\max}$. Consequently, the two CRW pairs arrive into a steady-state that can be predicted by a semi-analytic truncated model. These results were verified independently by the derivation of the weakly NL saturated behavior of the Ginzburg–Landau amplitude equation and by direct numerical simulations.

The Rayleigh model considered here is purely barotropic; thus, in order to prevent the flow from becoming become fully turbulent, a strong damping has been imposed on the dynamics. However, realistic jets in geophysical flows are generally both baroclinic and barotropic and do not experience transition to turbulence due to the wave-mean flow processes mentioned above (and due to the effect of rotation). A straightforward generalization of the NL Rayleigh model is a two-layer baroclinic model with a barotropic shear, in the presence of differential rotation (the latter can be represented by the β-plane approximation, for simplicity). We currently explore the nature of Rossby wave–wave interaction in such a model.

Finally, another possible extension of the work is based on HM05 CRW kernel generalization to the Rayleigh paradigm that can be applied to general smooth shear profiles. It is a straightforward step to include the nonlinear CRW interaction between such CRW kernels. Since the action at a distance is formulated in terms of Green functions, such generalization is relatively easy to implement in a numerical code. The CRW

kernel approach has been generalized further by Rabinovich et al. [35] to include linear interaction between modified Rossby-gravity kernel waves in shear flows in the presence of stratification. Similarly, we currently generalize the approach to be applicable to linearized shear flow in the presence of surface tension between immiscible fluids, and in the presence of the Lorentz force in plasma. The natural next step is to include the nonlinear modified CRW kernel interaction to the dynamics of such smooth shear flows and then to examine the weakly nonnormal–nonlinear feedback from the modified CRW kernel perspective.

Acknowledgments The authors would like to thank Nili Harnik for helpful discussions on this work. Eyal Heifetz is grateful to the hospitality of the Swedish International Meteorological Institute (IMI) and to the Israeli Science Foundation Grant 1084/06.

Appendix A: Nonlinear $k \Longleftrightarrow 2k$ CRW interaction

The nonlinear vorticity flux convergence, resulted from the interaction between a CRW pair of wavenumber k ($k + k = 2k$), can be written (in dimensional form) using (9) and (10b), as:

$$\begin{aligned}\left[-\frac{\partial(u_k q_k)}{\partial x}\right]_{2k}^{\pm b} &= \pm\frac{\partial}{\partial x}\left[\frac{\mathrm{e}^{-2kb}}{2}Q_k^2\cos\left(kx+\epsilon_k^{-b}\right)\cos\left(kx+\epsilon_k^{b}\right)\right]\\ &= \mp\frac{k}{2}\mathrm{e}^{-2kb}Q_k^2\sin\left[2\left(kx+\overline{\epsilon}_k\right)\right]\end{aligned} \tag{A1}$$

where $\overline{\epsilon}_k = \frac{1}{2}(\epsilon_k^{-b} + \epsilon_k^{b})$. Hence, due to the asymmetry of the induced streamwise velocity, a CRW pair of wavenumber k seeds nonlinearly anti-phased CRW pairs in wavenumber $2k$:

$$\begin{aligned}\frac{\partial}{\partial t}\left[Q_{2k}^{b}\cos\left(2kx+\epsilon_{2k}^{b}\right)\right] &= -\frac{k}{2}\mathrm{e}^{-2kb}Q_k^2\sin\left[2\left(kx+\overline{\epsilon}_k\right)\right]\\ &= -\frac{\partial}{\partial t}\left[Q_{2k}^{-b}\cos\left(2kx+\epsilon_{2k}^{-b}\right)\right]\end{aligned} \tag{A2}$$

Projecting (A2), first on the upper wave of $2k$ [i.e., multiplying Eq. (A2) by $\cos\left(2kx+\epsilon_{2k}^{b}\right)$ and integrate over wavelength, and next on the lower one], yields:

$$\dot{Q}_{2k}^{b} = -\frac{k}{2}\mathrm{e}^{-2kb}Q_k^2\sin\left(2\overline{\epsilon}_k-\epsilon_{2k}^{b}\right), \tag{A3a}$$

$$\dot{Q}_{2k}^{-b} = \frac{k}{2}\mathrm{e}^{-2kb}Q_k^2\sin\left(2\overline{\epsilon}_k-\epsilon_{2k}^{-b}\right) \tag{A3b}$$

Hence, for synchronous growth, $Q_{2k}^{b} = Q_{2k}^{-b} = Q_{2k}$, $2\overline{\epsilon}_k = \overline{\epsilon}_{2k}$, and

$$\dot{Q}_{2k} = \frac{k}{2}\mathrm{e}^{-2kb}Q_k^2\sin\left(\frac{\Delta\epsilon_{2k}}{2}\right) \tag{A4}$$

which is the dimensional form of the second term on the RHS of (12a). Repeating the procedure but projecting (A2) on the quadrature of the two waves [that is multiplying (A2) by $\sin(2kx+\epsilon_{2k}^{\pm b})$ and integrating over wavelength], and using the symmetry condition $2\overline{\epsilon}_k = \overline{\epsilon}_{2k}$, yields $\dot{\epsilon}_{2k}^{b} = \frac{k}{2}\mathrm{e}^{-2kb}\frac{Q_k^2}{Q_{2k}}\cos\left(\frac{\Delta\epsilon_{2k}}{2}\right) = -\dot{\epsilon}_{2k}^{-b}$, hence

$$\dot{\Delta\epsilon}_{2k} = k\mathrm{e}^{-2kb}\frac{Q_k^2}{Q_{2k}}\cos\left(\frac{\Delta\epsilon_{2k}}{2}\right) \tag{A5}$$

which is the dimensional form of the second term at the RHS of (12b).

Similarly, the backward nonlinear interaction ($2k - k = k$) can be written as:

$$\begin{aligned}&\left[-\frac{\partial\left[\left(u_k+u_{2k}\right)\left(q_k+q_{2k}\right)\right]}{\partial x}\right]_{k}^{\pm b}\\ &= \pm\frac{1}{2}\frac{\partial}{\partial x}\left[\left(q_k^{\mp b}\mathrm{e}^{-2kb}+q_{2k}^{\mp b}\mathrm{e}^{-4kb}\right)\left(q_k^{\pm b}+q_{2k}^{\pm b}\right)\right] \approx \pm\frac{1}{2}\frac{\partial}{\partial x}\left[\mathrm{e}^{-2kb}q_k^{\mp b}q_{2k}^{\pm b}\right]\end{aligned} \tag{A6}$$

Since the streamwise velocity associated with wavenumber $2k$ on the opposed boundary decays twice strongly than the one of wavenumber k, we neglect the former with respect to the latter. The term at the RHS then becomes: $\mp\frac{k}{4}\mathrm{e}^{-2kb}Q_kQ_{2k}\sin[kx+(\epsilon_{2k}^{\pm b}-\epsilon_k^{\mp b})]$, so that for the nonlinear evolution:

$$\frac{\partial}{\partial t}\left[Q_k\cos\left(kx+\epsilon_k^{b}\right)\right]=-\frac{k}{4}\mathrm{e}^{-2kb}Q_kQ_{2k}\sin\left[kx+\left(\epsilon_{2k}^{b}-\epsilon_k^{-b}\right)\right] \tag{A7a}$$

$$\frac{\partial}{\partial t}\left[Q_k\cos\left(kx+\epsilon_k^{-b}\right)\right]=\frac{k}{4}\mathrm{e}^{-2kb}Q_kQ_{2k}\sin\left[kx+\left(\epsilon_{2k}^{-b}-\epsilon_k^{b}\right)\right] \tag{A7b}$$

Projecting (A7) on the two waves and on their quadratures, together with the symmetry condition, $2\overline{\epsilon}_k=\overline{\epsilon}_{2k}$, yields after some algebra

$$\dot{Q}_k=-\frac{k}{4}\mathrm{e}^{-2kb}Q_kQ_{2k}\sin\left(\frac{\Delta\epsilon_{2k}}{2}\right) \tag{A8a}$$

$$\dot{\Delta\epsilon}_k=\frac{k}{2}\mathrm{e}^{-2kb}Q_{2k}\cos\left(\frac{\Delta\epsilon_{2k}}{2}\right) \tag{A8b}$$

which are the dimensional form of the second terms on the RHS of (11a, b), respectively.

Appendix B: Fixed point solutions

The steady-state solution and corresponding fixed point can be found by equating the RHS of (11) and (12) to zero,

$$\dot{Q}_k=\left\{[\sigma_k\sin(\Delta\epsilon_k)-r]-\frac{k}{2}\sigma_kQ_{2k}\sin\left(\frac{\Delta\epsilon_{2k}}{2}\right)\right\}Q_k=0, \tag{B1a}$$

$$\dot{\Delta\epsilon}_k=2\sigma_k[\cos(\Delta\epsilon_k)-f_k]+k\sigma_kQ_{2k}\cos\left(\frac{\Delta\epsilon_{2k}}{2}\right)=0, \tag{B1b}$$

$$\dot{Q}_{2k}=\left\{[\sigma_{2k}\sin(\Delta\epsilon_{2k})-r]+k\sigma_k\frac{Q_k^2}{Q_{2k}}\sin\left(\frac{\Delta\epsilon_{2k}}{2}\right)\right\}Q_{2k}=0, \tag{B2a}$$

$$\dot{\Delta\epsilon}_{2k}=2\sigma_{2k}[\cos(\Delta\epsilon_{2k})-f_{2k}]+2k\sigma_k\frac{Q_k^2}{Q_{2k}}\cos\left(\frac{\Delta\epsilon_{2k}}{2}\right)=0, \tag{B2b}$$

which results, after some algebra, the fixed points

$$(\Delta\epsilon_{2k})^{\mathrm{fp}}=2\tan^{-1}\left[\frac{r}{\sigma_{2k}(1+f_{2k})}\right], \tag{B3a}$$

$$(\Delta\epsilon_k)^{\mathrm{fp}}=\sin^{-1}\left[\left(f_k+\frac{\sigma_{2k}}{\sigma_k}(1+f_{2k})\right)\sin\frac{(\Delta\epsilon_{2k})^{\mathrm{fp}}}{2}\right]-\frac{(\Delta\epsilon_{2k})^{\mathrm{fp}}}{2}, \tag{B3b}$$

$$(Q_{2k})^{\mathrm{fp}}=2\frac{[f_k-\cos(\Delta\epsilon_k)^{\mathrm{fp}}]}{k\cos[\frac{(\Delta\epsilon_{2k})^{\mathrm{fp}}}{2}]}, \tag{B4a}$$

$$(Q_k)^{\mathrm{fp}}=\sqrt{\frac{[r-\sigma_{2k}\sin(\Delta\epsilon_{2k})^{\mathrm{fp}}]}{2[\sigma_k\sin(\Delta\epsilon_k)^{\mathrm{fp}}-r]}}(Q_{2k})^{\mathrm{fp}}. \tag{B4b}$$

To see this, note that from (B2a),

$$\frac{Q_k^2}{Q_{2k}}=\frac{[r-\sigma_{2k}\sin(\Delta\epsilon_{2k})]}{k\sigma_k\sin\left(\frac{\Delta\epsilon_{2k}}{2}\right)}, \tag{B5}$$

and from (B2b),

$$\frac{Q_k^2}{Q_{2k}} = \frac{\sigma_{2k}\left[f_k - \cos\left(\Delta\epsilon_{2k}\right)\right]}{k\sigma_k \cos\left(\frac{\Delta\epsilon_{2k}}{2}\right)}. \tag{B6}$$

Hence, comparing these two expressions, one finds

$$\frac{\left[r - \sigma_{2k}\sin\left(\Delta\epsilon_{2k}\right)\right]}{\sin\left(\frac{\Delta\epsilon_{2k}}{2}\right)} = \frac{\sigma_{2k}\left[f_k - \cos\left(\Delta\epsilon_{2k}\right)\right]}{\cos\left(\frac{\Delta\epsilon_{2k}}{2}\right)}. \tag{B7}$$

Plugging into (B7) the identities $\sin\left(\Delta\epsilon_2 k\right) = 2\sin\left(\frac{\Delta\epsilon_{2k}}{2}\right)\cos\left(\frac{\Delta\epsilon_{2k}}{2}\right)$ and $\cos\left(\Delta\epsilon_2 k\right) = 2\cos\left(\frac{\Delta\epsilon_{2k}}{2}\right)^2 - 1$, it can be easily shown that

$$\tan\left(\frac{\Delta\epsilon_{2k}}{2}\right) = \left[\frac{r}{\sigma_{2k}(1+f_{2k})}\right], \tag{B8}$$

so the fixed point solution indeed satisfies

$$\left(\Delta\epsilon_{2k}\right)^{\mathrm{fp}} = 2\tan^{-1}\left[\frac{r}{\sigma_{2k}(1+f_{2k})}\right]. \tag{B9}$$

In addition, from (B1a)

$$\sin\left(\frac{\Delta\epsilon_{2k}}{2}\right) = \frac{\sigma_k \sin\left(\Delta\epsilon_k\right) - r}{\frac{k}{2}\sigma_k Q_{2k}}, \tag{B10}$$

and from (B1b)

$$\cos\left(\frac{\Delta\epsilon_{2k}}{2}\right) = \frac{2\sigma_k[f_k - \cos\left(\Delta\epsilon_k\right)]}{k\sigma_k Q_{2k}}. \tag{B11}$$

Dividing these two expressions, one finds

$$\frac{\sin\left(\frac{\Delta\epsilon_{2k}}{2}\right)}{\cos\left(\frac{\Delta\epsilon_{2k}}{2}\right)} = \frac{\sigma_k \sin\left(\Delta\epsilon_k\right) - r}{\sigma_k\left(f_k - \cos\left(\Delta\epsilon_k\right)\right)}. \tag{B12}$$

Equation (B12) can be rearranged in the form

$$\sigma_k[\sin\left(\frac{\Delta\epsilon_{2k}}{2}\right)\cos\left(\Delta\epsilon_k\right) + \cos\left(\frac{\Delta\epsilon_{2k}}{2}\right)\cos\left(\Delta\epsilon_k\right)] = r\cos\left(\frac{\Delta\epsilon_{2k}}{2}\right) + f_k\sin\left(\frac{\Delta\epsilon_{2k}}{2}\right). \tag{B13}$$

Using the identity $\sin\left(\Delta\epsilon_k + \frac{\Delta\epsilon_{2k}}{2}\right) = \sin\left(\Delta\epsilon_k\right)\cos\left(\frac{\Delta\epsilon_{2k}}{2}\right) + \cos\left(\Delta\epsilon_k\right)\sin\left(\frac{\Delta\epsilon_{2k}}{2}\right)$, this can be written as

$$\sin\left(\Delta\epsilon_k + \frac{\Delta\epsilon_{2k}}{2}\right) = \sin\left(\frac{\Delta\epsilon_{2k}}{2}\right)\left[f_k + r\cot\left(\frac{\Delta\epsilon_{2k}}{2}\right)\right] = \sin\left(\frac{\Delta\epsilon_{2k}}{2}\right)\left[f_k + \frac{\sigma_{2k}}{\sigma_k}\left(1+f_{2k}\right)\right], \tag{B14}$$

where we have substituted expression (B8) to get the last equality. Given $\Delta\epsilon_{2k}^{\mathrm{fp}}$ from Eq. (B9), $\Delta\epsilon_k^{\mathrm{fp}}$ can than be calculated from (B14) by

$$\left(\Delta\epsilon_k\right)^{\mathrm{fp}} = \sin^{-1}\left[\left(f_k + \frac{\sigma_{2k}}{\sigma_k}(1+f_{2k})\right)\sin\frac{\left(\Delta\epsilon_{2k}\right)^{\mathrm{fp}}}{2}\right] - \frac{\left(\Delta\epsilon_{2k}\right)^{\mathrm{fp}}}{2}, \tag{B15}$$

which is the fixed point solution.

The expression for the steady-state amplitude Q_{2k} can be found directly from (B11) [or equivalently (B10)], given the expressions for $\Delta\epsilon_k^{\rm fp}$, $\Delta\epsilon_{2k}^{\rm fp}$, as

$$(Q_{2k})^{\rm fp} = 2\frac{[f_k - \cos{(\Delta\epsilon_k)^{\rm fp}}]}{k\cos[\frac{(\Delta\epsilon_{2k})^{\rm fp}}{2}]}. \tag{B16}$$

Finally, given all the fixed point expressions above, Q_k can be found directly from (B5) [or equivalently (B6)], which gives

$$(Q_k)^{\rm fp} = \sqrt{\frac{[r - \sigma_{2k}\sin{(\Delta\epsilon_{2k})^{\rm fp}}]}{2[\sigma_k \sin{(\Delta\epsilon_k)^{\rm fp}} - r]}}(Q_{2k})^{\rm fp}. \tag{B17}$$

Appendix C: Derivation of G–L amplitude equation

This appendix shows in detail the Ginzburg–Landau equation derivation. For the sake of completeness, we develop here the standard form of the Ginzburg–Landau equation, which takes into account slow spatial variations that result from the participant of wavenumbers at the vicinity of $k_{\rm max}$. However, in the truncated CRW model, only the interaction of the most unstable mode $k_{\rm max}$ is considered. Hence, for comparison, we later assume that the solution is entirely described by the maximal mode and neglect the slow spatial variations.[4]

When the departure from marginality is small, we can define ϵ as a small parameter so that $(k - k_{\rm max}) \equiv \epsilon\delta k$, and accordingly $(r_c - r) \equiv \epsilon^2\delta r$ (where δk and δr are assumed of order one). Then the modes in the vicinity of $k_{\rm max}$ can be written as:

$$\begin{aligned} q_k'(x, y, t) &= \left[q_k(y)\mathrm{e}^{\delta r T}\mathrm{e}^{ik_{\rm max}x}\right]\mathrm{e}^{i\delta kX}\mathrm{e}^{-b(\delta k)^2 T} + \text{c.c.} \\ &\approx q'_{k_{\rm max}}\mathrm{e}^{i\delta kX}\mathrm{e}^{-b(\delta k)^2 T} + \text{c.c.} \end{aligned} \tag{C1}$$

where $X \equiv \epsilon x$, $T \equiv \epsilon^2 t$. Hence, the unstable modes have approximately the structure of the most unstable one with an envelope that varies slowly in the streamwise direction, and decays, even slower, with time. The general weakly nonlinear solution is therefore expected to be a function of (x, X, T, y) so that all differential operators are expressed in the form $\frac{\partial}{\partial x} \to \frac{\partial}{\partial x} + \epsilon\frac{\partial}{\partial X}$ and $\frac{\partial}{\partial t} \to \epsilon^2\frac{\partial}{\partial T}$. In order to proceed with a classical weakly nonlinear solution calculation, we adopt a continuous vorticity profile that closely approximates the step profile, as that given by Eq. (19).

Weakly nonlinear solutions of (A1) are assumed to be represented by the following series expansions

$$\begin{aligned} q &= q_0 + \epsilon q_1 + \epsilon^2 q_2 + \epsilon^3 q_3 + \cdots; \qquad \psi = \psi_0 + \epsilon\psi_1 + \epsilon^2\psi_2 + \epsilon^3\psi_3 + \cdots \\ u &= u_0 + \epsilon u_1 + \epsilon^2 u_2 + \epsilon^3 u_3 + \cdots; \qquad v = \epsilon v_1 + \epsilon^2 v_2 + \epsilon^3 v_3 + \cdots, \end{aligned}$$

where q_0, u_0 and ψ_0 are the mean flow quantities $\overline{q}$, $\overline{U}$ and $\overline{\psi}$, respectively. With the special parameters chosen above, the next order ϵ solution is the marginal state, written as

$$\psi_1(x, X, T, y) = A(X, T)\tilde{\psi}_1(y)\mathrm{e}^{ik_c x} + \text{c.c.} \tag{C2}$$

where $\tilde{\psi}_1(y)$ is the normalized eigenfunction of the most unstable mode and A is the amplitude.

In the following derivations, we use the subscript notation to denote partial derivatives ($\partial_y \equiv \frac{\partial}{\partial y}$, $\partial_T \equiv \frac{\partial}{\partial T}$ and so on). Adopting the expansions described here and applying them directly into the vorticity Eq. (1) and the diagnostic expressions $\nabla^2\psi = q$, $u = -\partial_y\psi$, $v = \partial_x\psi$, reveals

[4] The slow variation of the amplitude in the streamwise direction becomes significant only for length scales which are much larger than the typical wavelength scale $\lambda_{\rm max} = 2\pi/k_{\rm max}$. Hence, for comparison with the truncated CRW model, we exclude slow spatial variations, bearing in mind that the focus is on length scales at the order of $\lambda_{\rm max}$.

$$\left[\epsilon^2\partial_T + (u_0+\epsilon u_1+\epsilon^2u_2+\epsilon^3u_3)(\partial_x+\epsilon\partial_X) + (\epsilon v_1+\epsilon^2v_2+\epsilon^3v_3)\partial_y\right]\left(q_0+\epsilon q_1+\epsilon^2q_2+\epsilon^3q_3\right)$$
$$= -(r_c-\epsilon^2r_2)\left(\epsilon q_1+\epsilon^2q_2+\epsilon^3q_3\right), \tag{C3}$$
$$\left(\partial_x^2+2\epsilon\partial_x\partial_X+\epsilon^2\partial_X^2+\partial_y^2\right)(\psi_0+\epsilon\psi_1+\epsilon^2\psi_2+\epsilon^3\psi_3) = q_0+\epsilon q_1+\epsilon^2q_2+\epsilon^3q_3, \tag{C4}$$
$$u_0+\epsilon u_1+\epsilon^2u_2+\epsilon^3u_3 = -\partial_y\left(\psi_0+\epsilon\psi_1+\epsilon^2\psi_2+\epsilon^3\psi_3\right), \tag{C5}$$
$$\epsilon v_1+\epsilon^2v_2+\epsilon^3v_3 = (\partial_x+\epsilon\partial_X)\left(\epsilon\psi_1+\epsilon^2\psi_2+\epsilon^3\psi_3\right). \tag{C6}$$

The next proceeder is to solve Eqs. (C3–C6) order by order in powers of ϵ, impose a solvability condition and arrive at an amplitude equation. Note that at each order, we solve a series of forced boundary value problems which are determined numerically using a Chebyshev decomposition.

C.1 Order 0

Because $q_0 = \overline{q}(y)$, it follows that the leading order equations reduce to the mean streamfunction $\psi_0(y)$ and corresponding mean wind, $u_0(y)$, as solutions to

$$\partial_y^2\psi_0 = q_0 \tag{C7}$$

where the mean wind is specifically given by $u_0 = -\partial_y\psi_0$. Because q_0 depends upon y only, there is no corresponding vertical velocity function v_0 at leading order. These are the same mean states perturbed in the linear theory section before.

C.2 Order ϵ

At next order in ϵ the Eqs. (C3–C6) are

$$u_0\partial_xq_1+v_1\partial_yq_0 = -r_cq_1, \qquad (\partial_y^2+\partial_x^2)\psi_1 = q_1, \tag{C8}$$
$$u_1 = \partial_y\psi_1, \qquad v_1 = \partial_x\psi_1,$$

with the boundary condition $\psi_1(y\to\pm L)\to 0$. Because this expansion procedure is built around the marginal solutions with a critical wavenumber $k = k_c$, solutions of the form

$$\begin{pmatrix} q_1\\ \psi_1\\ u_1\\ v_1\end{pmatrix} = \begin{pmatrix} q_{11}\\ \psi_{11}\\ u_{11}\\ v_{11}\end{pmatrix}\mathrm{e}^{ik_cx}+\text{c.c.} \tag{C9}$$

are assumed. The above equations may be combined into a single one for ψ_{11}

$$\mathcal{L}\psi_{11} = 0, \qquad \mathcal{L}\equiv\partial_y^2-k_c^2+\frac{ik_cq_{0y}}{ik_cu_0+r_c}, \tag{C10}$$

The solutions of (C10) in which $\psi_{11}\to 0$ as $y\to\pm L$ are the eigenfunctions describing the marginal state. If we denote $\tilde{\psi}_{11}(y)$ as the normalized base eigenfunction that satisfy $\lim_{L\to\infty}\int_{-L}^{L}|\tilde{\psi}_{11}|^2\mathrm{d}y = 1$, then the general solution for ψ_{11} is given by

$$\psi_{11}(X,T,y) = A(X,T)\tilde{\psi}_{11}(y)+\text{c.c.} \tag{C11}$$

where the arbitrary amplitude A is yet to be determined. It follows therefore that

$$q_{11} = A\tilde{q}_{11}, \qquad u_{11} = A\tilde{u}_{11}, \qquad v_{11} = A\tilde{v}_{11}; \tag{C12}$$

where

$$\tilde{q}_{11} = (\partial_y^2-k_c^2)\tilde{\psi}_{11}, \qquad \tilde{u}_{11} = -\partial_y\tilde{\psi}_{11}, \qquad \tilde{v}_{11} = ik_c\tilde{\psi}_{11}. \tag{C13}$$

Before proceeding we note the following: multiplying (C10) by a function $\psi^\dagger$ and integrating between $\pm L$ gives

$$\int_{-L}^{L} \psi^\dagger \mathcal{L}\psi_{11} \mathrm{d}y = \left[\psi^\dagger \partial_y \psi_{11}\right]_{y\to -L}^{y\to L} - \left[\psi_{11}\partial_y \psi^\dagger\right]_{y\to -L}^{y\to L} + \int_{-L}^{L} \psi_{11}\mathcal{L}\psi^\dagger \mathrm{d}y = 0, \tag{C14}$$

As long as $\psi_{11}(y \to \pm L) = 0$ and $\psi^\dagger(y \to \pm L) = 0$ it must follow that $\int_{-L}^{L} \psi_{11}\mathcal{L}\psi^\dagger \mathrm{d}y = 0$, and this statement is trivially satisfied for $\psi^\dagger = \psi_{11}$.

Henceforth, the integral product of two quantities shall be symbolically represented by $\langle fg\rangle \equiv \int_{-L}^{L} (f \cdot g)\, \mathrm{d}y$

C.3 Order ϵ^2

The equations at the next order are

$$u_0\partial_x q_2 + u_1\partial_x q_1 + u_0\partial_X q_1 + v_2\partial_y q_0 + v_1\partial_y q_1 = -r_c q_2 \tag{C15}$$

$$(\partial_y^2 + \partial_x^2)\psi_2 + 2\partial_X\partial_x\psi_1 = q_2, \tag{C16}$$

$$u_2 = -\partial_y\psi_2 v_2 = \partial_x\psi_2 + \partial_X\psi_1. \tag{C17}$$

We can combine the above set of equations into a single one for ψ_2

$$\begin{aligned}&[(u_0\partial_x + r_c)\left(\partial_y^2 + \partial_x^2\right) + q_{0y}\partial_x]\psi_2 = \\ &-u_1\partial_x q_1 - v_1\partial_y q_1 - u_0\partial_X q_1 - 2\,(u_0\partial_x + r_c)\,\partial_X\partial_x\psi_1 - q_{0y}\partial_X\psi_1.\end{aligned} \tag{C18}$$

with the boundary condition $v_2 \to 0$ as $y \to \pm L$.

Note that the form of Eq. C18 is of a linear operator acting on ψ_2 with known source terms on its RHS. Analysis of these terms shows that they must be proportional to $\mathrm{e}^{\pm ik_c x}$, $\mathrm{e}^{\pm 2ik_c x}$, or independent of x. Defining the vector $\mathbf{V}_2 \equiv [q_2, \psi_2, u_2, v_2]^{\mathrm{T}}$ (where the superscript "T" denotes the vector transpose), the general solution at this order may be written as

$$\mathbf{V}_2 = \mathbf{V}_{20} + \left(\mathbf{V}_{21}\mathrm{e}^{ik_c x} + \mathbf{V}_{22}\mathrm{e}^{i2k_c x} + \mathrm{c.c.}\right), \tag{C19}$$

where $\mathbf{V}_{2i} \equiv [q_{2i}(y), \psi_{2i}(y), u_{2i}(y), v_{2i}(y)]^{\mathrm{T}}$, with $i = 0, 1, 2$. The RHS of (C18) can thus be rewritten in the form

$$[(u_0\partial_x + r_c)\left(\partial_y^2 + \partial_x^2\right) + q_{0y}\partial_x]\psi_2 = \mathcal{R}_{20} + \left[\mathcal{R}_{21}\mathrm{e}^{ik_c x} + \mathcal{R}_{22}\mathrm{e}^{i2k_c x} + \mathrm{c.c.}\right], \tag{C20}$$

where

$$\mathcal{R}_{20} = |A|^2 ik_c\partial_y\left(\tilde{q}_{11}\tilde{\psi}_{11}^* - \tilde{q}_{11}^*\tilde{\psi}_{11}\right)$$

$$\mathcal{R}_{22} = A^2 ik_c\left(\tilde{q}_{11}\tilde{\partial}_y\psi_{11} - \tilde{\psi}_{11}\partial_y\tilde{q}_{11}\right)$$

and

$$\mathcal{R}_{21} = -A_X\left[(ik_c u_0 + r_c)2ik_c + q_{0y}\right]\tilde{\psi}_{11} - A_X u_0\tilde{q}_{11}. \tag{C21}$$

with the notation $A_X \equiv \partial_X A$. In order to establish the solutions to the y-structure functions associated with each Fourier component, we re-express the general solution form in terms of ψ_2 only

$$\psi_2 = \psi_{20} + \left(\psi_{21}\mathrm{e}^{ik_c x} + \psi_{22}\mathrm{e}^{i2k_c x} + \mathrm{c.c.}\right), \tag{C22}$$

and address each Fourier component individually.

For the zeroth Fourier component, we have $\psi_{20} = |A|^2\tilde{\psi}_{20}$ in which $\tilde{\psi}_{20}$ is the solution of

$$\tilde{q}_{20} = \partial_y^2\tilde{\psi}_{20} = \frac{ik_c}{r_c}\partial_y\left(\tilde{q}_{11}\tilde{\psi}_{11}^* - \tilde{q}_{11}^*\tilde{\psi}_{11}\right), \tag{C23}$$

where the superscript "$*$" denotes complex conjugate. Since (C23) is written in exact differential form, it follows that that $u_{20} = |A|^2\tilde{u}_{20}$ with

$$\tilde{u}_{20} = -\frac{ik_c}{r_c}\left(\tilde{q}_{11}\tilde{\psi}_{11}^* - \tilde{q}_{11}^*\tilde{\psi}_{11}\right). \tag{C24}$$

Consistently, it also follows that $v_{20} = 0$. Note that (C23) is the equation establishing the amount of mean flow adjustment that occurs due to classical wave–mean flow interaction. It measures the balance between the "dissipation" due to the vorticity forcing ($r_c\partial_y^2\psi_{20}$) and the convergence of the momentum flux (embodied by $\mathcal{R}_{20}$).

For the $2k_c$ Fourier component, we find that $\psi_{22} = A^2\tilde{\psi}_{22}$ in which $\tilde{\psi}_{22}$ is the solution of

$$\mathcal{L}_2\tilde{\psi}_{22} = \left[\partial_y^2 - (2k_c)^2 + \frac{(2ik_c)q_{0y}}{u_0(2ik_c) + r_c}\right]\tilde{\psi}_{22} = \frac{ik_c}{u_0(2ik_c) + r_c}\left(\tilde{q}_{11}\partial_y\tilde{\psi}_{11} - \tilde{\psi}_{11}\partial_y\tilde{q}_{11}\right), \tag{C25}$$

in which $\tilde{\psi}_{22} \to 0$ as $y \to \pm L$. It follows that

$$q_{22} = A^2\tilde{q}_{22}, \qquad u_{22} = A^2\tilde{u}_{22}, \qquad v_{22} = A^2\tilde{v}_{22};$$

where

$$\tilde{q}_{22} = (\partial_y^2 - 4k_c^2)\tilde{\psi_{22}}, \qquad \tilde{u}_{22} = -\partial_y\tilde{\psi}_{22}, \qquad \tilde{v}_{22} = i2k_c\tilde{\psi}_{22}.$$

For the k_c component, it follows that $\psi_{21} = A_X\tilde{\psi}_{21}$ in which $\tilde{\psi}_{21}$ is the solution of

$$\mathcal{L}\tilde{\psi}_{21} = -\left(2ik_c + \frac{q_{0y}}{u_0ik_c + r_c}\right)\tilde{\psi}_{11} - \frac{u_0\tilde{q}_{11}}{u_0ik_c + r_c}. \tag{C26}$$

Since the operator on $\tilde{\psi}_{21}$ appearing on the LHS of (C26) is the same as the lowest order linear operator at $O(\epsilon)$, in order for a solution to exist in which $\psi_{21} \to 0$ as $y \to \pm L$, the RHS of (C26) must project onto the nullspace of the operator $\mathcal{L}$. However, this is satisfied by virtue of the fact we are expanding around the marginal state of the system. In other words, by the choice of parameters we have started with, it follows automatically that

$$\left\langle \psi^\dagger\mathcal{L}\tilde{\psi}_{21}\right\rangle = -\left\langle \psi^\dagger\left[\left(2ik_c + \frac{q_{0y}}{u_0ik_c + r_c}\right)\tilde{\psi}_{11} + \frac{u_0\tilde{q}_{11}}{u_0ik_c + r_c}\right]\right\rangle = 0, \tag{C27}$$

recalling that $\psi^\dagger = \tilde{\psi}_{11}$. It similarly follows that the remainder quantities are constructed out of $\tilde{\psi}_{21}$ according to,

$$\begin{aligned} &q_{21} = A_X\tilde{q}_{21}, \qquad u_{21} = A_X\tilde{u}_{21}, \qquad v_{21} = A_X\tilde{v}_{21};\\ &\tilde{q}_{21} = (\partial_y^2 - k_c^2)\tilde{\psi}_{21}, \qquad \tilde{u}_{21} = -\partial_y\tilde{\psi}_{21}, \qquad \tilde{v}_{21} = ik_c\tilde{\psi}_{21} + \tilde{\psi}_{11}. \end{aligned}$$

C.4 Order ϵ^3: Solvability and amplitude equation

The equations at this order are

$$\partial_T q_1 + u_2\partial_x q_1 + u_1\partial_X q_1 + u_1\partial_x q_2 + u_0\partial_x q_3 + u_0\partial_X q_2 + v_1\partial_y q_2 + v_2\partial_y q_1 + v_3\partial_y q_0 = -r_c q_3 - r_2 q_1 \tag{C28}$$

$$(\partial_y^2 + \partial_x^2)\psi_3 + 2\partial_x\partial_X\psi_2 + \partial_X^2\psi_1 = q_3 \tag{C29}$$

$$u_3 = -\partial_y\psi_3 \tag{C30}$$

$$v_3 = \partial_x\psi_3 + \partial_X\psi_2 \tag{C31}$$

Solutions to this set of equations will have the general form

$$\mathbf{V}_3 = \mathbf{V}_{30} + \left(\mathbf{V}_{31}e^{ik_cx} + \mathbf{V}_{32}e^{i2k_cx} + \mathbf{V}_{33}e^{i3k_cx} + \text{c.c.}\right), \tag{C32}$$

where $\mathbf{V}_{3i} \equiv [q_{3i}(y), \psi_{3i}(y), u_{3i}(y), v_{3i}(y)]^{\mathrm{T}}$. Instead of establishing this general solution, we seek to sort out a partial solution by establishing a necessary condition for the existence of a solution. We combine (C28–C31) into a single equation for ψ_3

$$[(u_0\partial_x + r_c)(\partial_y^2 + \partial_x^2) + q_{0y}\partial_x]\psi_3 = \mathcal{R}_{30} + [\mathcal{R}_{33}\mathrm{e}^{i3k_cx} + \mathcal{R}_{32}\mathrm{e}^{i2k_cx} + \mathcal{R}_{31}\mathrm{e}^{ik_cx} + \text{c.c.}] \tag{C33}$$

For our purposes, it is enough to analyze $\mathcal{R}_{31}$ as it will be this term that governs the existence of a solution at this order. Since we have the ansatz

$$\psi_3 = \psi_{30} + \left(\psi_{33}\mathrm{e}^{i3k_cx} + \psi_{32}\mathrm{e}^{i2k_cx} + \psi_{31}\mathrm{e}^{ik_cx} + \text{c.c.}\right) \tag{C34}$$

we are concerned with the development of ψ_{31}. The equation governing its form is

$$\mathcal{L}\psi_{31} = \frac{\mathcal{R}_{31}}{ik_cu_0 + r_c}, \tag{C35}$$

where the operator $\mathcal{L}$ is as given in (C10) and where

$$\begin{aligned}\mathcal{R}_{31} = {} & -A_T\tilde{q}_{11} + r_2A\tilde{q}_{11} - A_{XX}[-2u_0k_c^2\tilde{\psi}_{21} + ik_cu_0\tilde{\psi}_{11} + u_0\tilde{q}_{21} + q_{0y}\tilde{\psi}_{21}] \\ & -A|A|^2[-ik_c\tilde{u}_{22}\tilde{q}_{11}^* + 2ik_c\tilde{q}_{22}\tilde{u}_{11}^* + \tilde{v}_{11}^*\partial_y\tilde{q}_{22} + \tilde{v}_{22}\partial_y\tilde{q}_{11}^* + ik_c\tilde{u}_{20}\tilde{q}_{11} + \tilde{v}_{11}\partial_y\tilde{q}_{20}].\end{aligned} \tag{C36}$$

In order for ψ_{31} to be able to satisfy the boundary condition $ik_c\psi_{31} \to 0$ as $y \to \pm L$, it must be that $\mathcal{R}_{31}$ lies in the null space of the operator $\mathcal{L}$ (just as it was the case for the solution for ψ_{21}). This means that it must follow that

$$\left\langle \psi^\dagger \frac{\mathcal{R}_{31}}{ik_cu_0 + r_c} \right\rangle = 0. \tag{C37}$$

This may be satisfied if the amplitude A satisfies the Complex Ginzburg–Landau equation

$$\frac{\partial A}{\partial T} = \delta r A - \gamma A_{XX} - (\beta_{2\mathrm{k}} + \beta_0)A|A|^2 \tag{C38}$$

where

$$\begin{aligned}\gamma &= \frac{1}{\left\langle \frac{\psi^\dagger\tilde{q}_{11}}{ik_cu_0+r_c} \right\rangle} \left\langle \frac{\psi^\dagger\left(-2u_0k_c^2\tilde{\psi}_{21} + ik_cu_0\tilde{\psi}_{11} + u_0\tilde{q}_{21} + q_{0y}\tilde{\psi}_{21}\right)}{ik_cu_0 + r_c} \right\rangle, \\ \beta_{2\mathrm{k}} &= \frac{1}{\left\langle \frac{\psi^\dagger\tilde{q}_{11}}{ik_cu_0+r_c} \right\rangle} \left\langle \frac{\psi^\dagger\left(-ik_c\tilde{u}_{22}\tilde{q}_{11}^* + 2ik_c\tilde{q}_{22}\tilde{u}_{11}^* + \tilde{v}_{11}^*\partial_y\tilde{q}_{22} + \tilde{v}_{22}\partial_y\tilde{q}_{11}^*\right)}{ik_cu_0 + r_c} \right\rangle, \\ \beta_0 &= \frac{1}{\left\langle \frac{\psi^\dagger\tilde{q}_{11}}{ik_cu_0+r_c} \right\rangle} \left\langle \frac{\psi^\dagger\left(ik_c\tilde{u}_{20}\tilde{q}_{11} + \tilde{v}_{11}\partial_y\tilde{q}_{20}\right)}{ik_cu_0 + r_c} \right\rangle.\end{aligned}$$

For comparison with the truncated CRW model, which involves only the most unstable mode, we set $A_{xx} = 0$ as explained above. In addition, for a time independent mean flow, $\beta_0 = 0$ since $\tilde{u}_{20} = \tilde{q}_{20} = 0$ by definition. Hence, keeping only the wave–wave nonlinear interaction $k \Longleftrightarrow 2k$ represented by the term β_{2k}, the Ginzburg–Landau equation is simplified to:

$$\frac{\partial A}{\partial T} = \delta r A - \beta_{2\mathrm{k}}A|A|^2. \tag{C39}$$

References

1. Bretherton, F.P.: Baroclinic instability, the short wave cutoff in terms of potential vorticity. Q. J. R. Meteor. Soc. **92**, 335–345 (1966)
2. Hoskins, B.J., McIntyre, M.E., Robertson, A.W.: On the use and significance of isentropic potential vorticity maps. Q. J. R. Meteor. Soc. **111**, 877–946 (1985)
3. Davies, H.C., Bishop, C.H.: Eady edge waves and rapid development. J. Atmos. Sci. **51**, 1930–1946 (1994)
4. Bishop, C.H., Heifetz, E.: Apparent absolute instability and the continuous spectrum. J. Atmos. Sci. **57**, 3592 (2000)
5. Heifetz, E., Bishop, C.H., Hoskins, B.J., Alpert, P.: Counter-propagating Rossby waves in barotropic rayleigh model of shear instability. Q. J. R. Meteor. Soc. **125**, 2835–2853 (1999)
6. Badger, J., Hoskins, B.J.: Simple initial value problems and mechanisms for baroclinic growth. Q. J. R. Meteor. Soc. **58**, 38–49 (2001)
7. Heifetz, E., Bishop, C.H., Hoskins, B.J., Methven, J.: The counter-propagating Rossby wave perspective on baroclinic instability Part I: mathematical basis. Q. J. R. Meteor. Soc. **130**, 211–232 (2004)
8. de Vries, H., Opsteegh, J.D.: Optimal perturbations in the Eady model: resonance versus PV unshielding. J. Atmos. Sci. **62**, 492–505 (2005)
9. Røsting, B., Kristjánsson, J.E.: The usefulness of piecewise potential vorticity inversion. J. Atmos. Sci. **69**, 934–941 (2012)
10. Iga, K.: Shear instability as a resonance between neutral waves hidden in a shear flow. J. Fluid Mech. **715**, 452–476 (2013)
11. Biancofiore, L., Gallaire, F.: The influence of shear layer thickness on the stability of confined two dimensional wakes. Phys. Fluids **23**, 034103 (2012)
12. Heifetz, E., Methven, J.: Relating optimal growth to counter-propagating Rossby waves in shear instability. Phys. Fluids **17**, 064107 (2005)
13. Pedlosky, J.: Finite-amplitude baroclinic waves. J. Atmos. Sci. **27**, 15–30 (1970)
14. Martius, O., Schwierz, C., Davies, H.C.: Tropopause-level waveguides. J. Atmos. Sci. **67**, 866–879 (2010)
15. Majda, A.J., Biello, J.A.: The nonlinear interaction of barotropic and equatorial baroclinic Rossby waves. J. Atmos. Sci. **60**, 1809–1821 (2003)
16. Chelton, D.B., Schlax, M.G., Samelson, R.M., de Szoeke, R.A.: Global observations of large oceanic eddies. Geophys. Res. Lett. **34**, L15606 (2007)
17. Lovelace, R.V.E., Romanova, M.M.: Rossby wave instability in astrophysical discs. Fluid Dyn. Res. **46**, 041401 (2014)
18. Rayleigh, L.: On the stability, or instability, of certain fluid motions. Proc. Lond. Math. Soc. **9**, 57–70 (1880)
19. Lin, S.-J., Pierrehumbert, R.T.: Does Ekman Friction suppress baroclinic instability?. J. Atmos. Sci. **45**, 2920–2933 (1988)
20. Antar, B.N., Fowlis, W.W.: Eigenvalues of a baroclinic stability problem with Ekman damping. J. Atmos. Sci. **37**, 1399–1404 (1980)
21. Dritschel, D.: On the stabilization of a two-dimensional vortex strip by adverse shear. J. Fluid Mech. **206**, 193–221 (1989)
22. Henry, D., Ivanov, R.: One-dimensional weakly nonlinear model equations for Rossby waves. Discret. Contin. Dyn. Syst. **34**, 3025–3034 (2014)
23. Graef, F.: Second order nonlinear interactions among Rossby waves. Atmósfera **7**, 89–103 (1993)
24. Vanneste, J.: A nonlinear critical layer generated by the interaction of free Rossby waves. J. Fluid Mech. **371**, 319–344 (1998)
25. Ho, C.M., Huerre, P.: Perturbed free shear layers. Annu. Rev. Fluid Mech. **16**, 365–422 (1984)
26. Baggett, J.S., Trefethen, L.N.: A mostly linear model of transition to turbulence. Phys. Fluids **7**, 833 (1995)
27. Umurhan, O.M., Regev, O.: Hydrodynamic stability of rotationally supported flows: linear and nonlinear 2D shearing box results. Astron. Astrophys. **427**, 855–872 (2004)
28. Canuto, C., Hussaini, M.Y., Quarteroni, A., Zang, T.A.: Spectral Methods in Fluid Dynamics. Springer, Berlin (1988)
29. Vallis, G.K.: Atmospheric and Oceanic Fluid Dynamics. Cambridge University Press, Cambridge (2006)
30. Eady, E.T.: Long waves and cyclone waves. Tellus **1**, 33–52 (1949)
31. Charney, J.G., Stern, M.E.: On the stability of internal baroclinic jets in a rotating atmosphere. J. Atmos. Sci. **19**, 159–172 (1962)
32. Phillips, N.A.: The general circulation of the atmosphere: a numerical experiment. Q. J. R. Meteorol. Soc., **82**, 535–539 (1956)
33. Harnik, N., Dritschel, D.G., Heifetz, E.: On the equilibration of asymmetric barotropic instability. Q. J. R. Meteorol. Soc. **140**, 2444–2464 (2014)
34. Dritschel, D.G., Scott, R.K.: Jet sharpening by turbulent mixing. Philos. Trans. A. Math. Phys. Eng. Sci. **369**, 754–770 (2011)
35. Rabinovich, A., Umurhan, O.M., Harnik, N., Lott, F., Heifetz, E.: Vorticity inversion and action-at-a-distance instability in stably stratified shear flow. J. Fluid Mech. **670**, 301–325 (2011)